Journal of Biomolecular NMR, 10 (1997) 107–118
KLUWER/ESCOM

J-Bio NMR 456

Application of H(N)CA,CO-E.COSY experiments for calibrating the ϕ angular dependences of vicinal couplings $J(C'_{i-1},H^{\alpha}_i)$, $J(C'_{i-1},C^{\beta}_i)$ and $J(C'_{i-1},C'_i)$ in proteins

Frank Löhr, Markus Blümel, Jürgen M. Schmidt and Heinz Rüterjans*

Institut für Biophysikalische Chemie, Johann Wolfgang Goethe Universität Frankfurt am Main, Biozentrum N230, Marie-Curie-Strasse 9, D-60439 Frankfurt, Germany

Received 10 March 1997
Accepted 8 April 1997

Keywords: Vicinal coupling constants; ϕ Torsion angle; Karplus parametrization; *Desulfovibrio vulgaris* flavodoxin; Isotopic labelling

Summary

A triple-resonance NMR technique suitable for the determination of carbonyl-related couplings in polypeptide systems is introduced. The application of three novel pulse sequences to uniformly $^{13}C/^{15}N$-enriched proteins yields E.COSY-like multiplet patterns exhibiting either one of the $^3J(C'_{i-1},H^{\alpha}_i)$, $^3J(C'_{i-1},C^{\beta}_i)$ and $^3J(C'_{i-1},C'_i)$ coupling constants in the indirectly detected $^{13}C'$ dimension, depending on the passive spin selected. The experiments are demonstrated with oxidized flavodoxin from *Desulfovibrio vulgaris*. On the basis of the J-values measured and the backbone ϕ-angles derived from a high-resolution X-ray structure of the protein, the three associated Karplus equations were reparametrized. The root-mean-square differences between the experimental coupling constants and those predicted by the optimized Karplus curves are 0.41, 0.33 and 0.32 Hz for $^3J(C'_{i-1},H^{\alpha}_i)$, $^3J(C'_{i-1},C^{\beta}_i)$ and $^3J(C'_{i-1},C'_i)$, respectively. The results are compared with the Karplus parameters previously published for the same couplings.

Introduction

Information from homonuclear and heteronuclear ^3J coupling constants is now routinely included in protein structure determination (Bax et al., 1994; Biamonti et al., 1994; Case et al., 1994; Eberstadt et al., 1995). The conversion of coupling constants into local conformation is based on the empirical relation by Karplus (1959,1963):

$$^3J(\theta) = A_k \cos^2 \theta + B_k \cos \theta + C_k \qquad (1)$$

where the dihedral angle θ is subtended by three consecutive covalent bonds that connect the pair k of coupled nuclei, and the coefficients A_k, B_k and C_k are given in Hz. Obviously, the utility of vicinal coupling constants in dihedral-angle calculation depends on both the quality of experimental data and the reliability of available Karplus coefficients. For peptide systems, parametrizations of Eq. 1 originally emerged from quantum-mechanical approaches or from experiments on either freely rotating or conformationally constrained small model molecules (Hansen et al., 1975; Bystrov, 1976; Fischman et al., 1980). Alternatively, empirical coefficients for vicinal $^1H,^1H$, $^1H,^{13}C$ and $^1H,^{15}N$ couplings in peptides were calibrated based on known structures (DeMarco et al., 1978a,b,c; DeMarco and Llinás, 1979). Recent parametrizations of the dihedral-angle dependence of $^3J(H^N,H^{\alpha})$ in various proteins refer to high-resolution X-ray structures (Pardi et al., 1984; Ludvigsen et al., 1991; Vuister and Bax, 1993; Wang and Bax, 1996), taking advantage of the large number of data points simultaneously obtained from a single protein spectrum. The coefficients thus determined include the contributions from thermal torsional-angle fluctuations typically encountered in proteins (Hoch et al., 1985; Brüschweiler and Case, 1994).

According to Eq. 1, a particular J-value specifies up to four dihedral angles. Thus, the derivation of correct angular restraints requires that a set of coupling constants associated with the same torsion angle be measured in order to resolve the inherent degeneracy. In the following,

*To whom correspondence should be addressed.

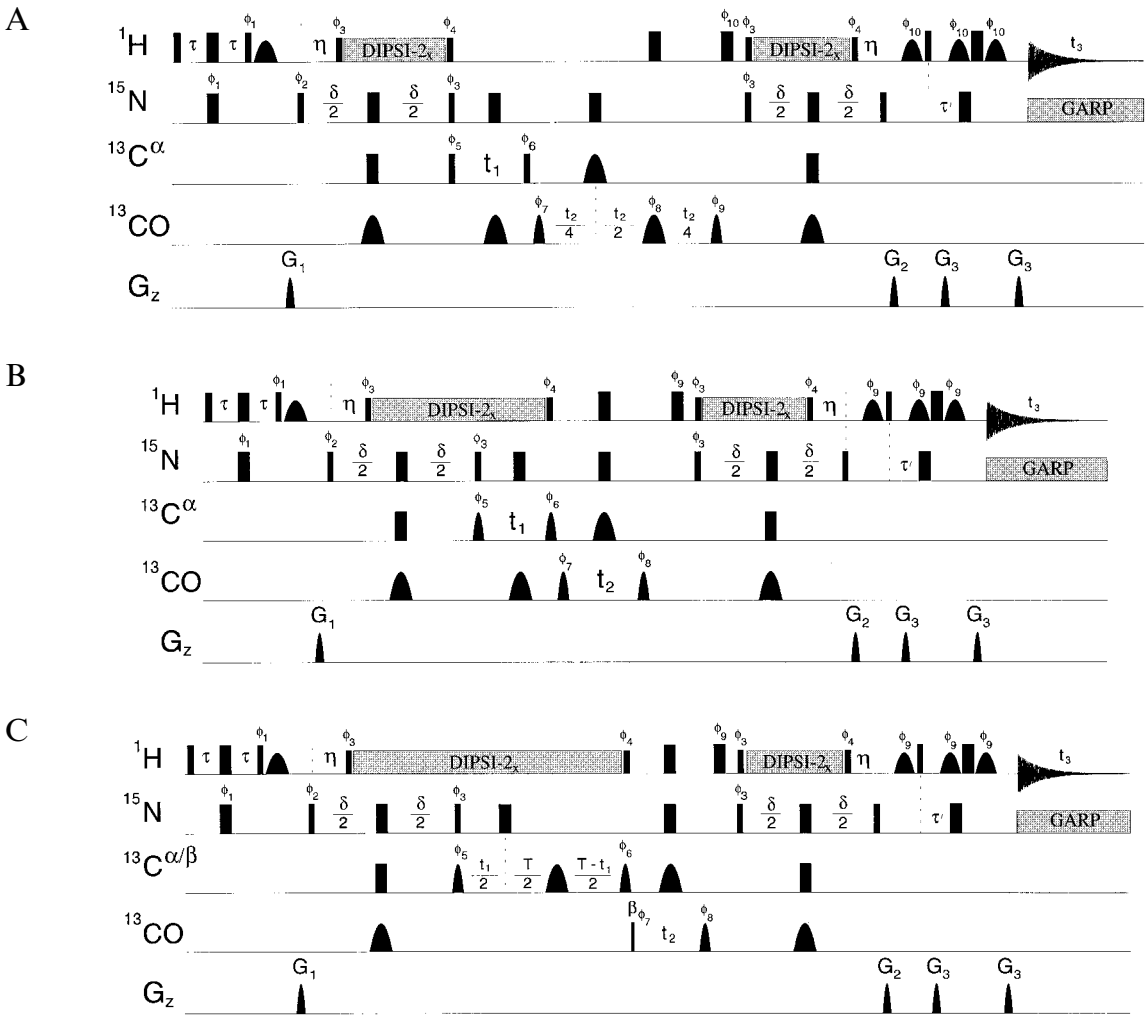

Fig. 1. Water flip-back versions of the H(N)CA,CO-E.COSY pulse sequence for measuring (A) $^3J(C'_{i-1},H_i^{\alpha})$, (B) $^3J(C'_{i-1},C_i^{\beta})$ and (C) $^3J(C'_{i-1},C'_i)$ coupling constants. The proton carrier frequency is placed onto the water resonance throughout the sequences. The carbon carrier is positioned at 58 ppm in schemes A and C and at 59 ppm in B, being temporarily switched to 176 ppm during t_2 evolution periods. Unless indicated explicitly, pulse phases are adjusted to the +x axis. Narrow and wide bars denote rectangular pulses with 90° and 180° flip angles, respectively, except for the pulse labelled β (sequence C), which has a flip angle of 35° corresponding to a duration of 54 μs. The rf field strengths are typically 4.5 and 0.76 kHz for the ^{1}H DIPSI-2 sequences (Shaka et al., 1988) including the flanking 90° pulses and GARP-1 (Shaka et al., 1985) nitrogen decoupling during acquisition, respectively. Water-selective Gaussian-shaped 90° pulses have a duration of 2.5 ms. The widths of rectangular pulses applied to α-carbons are adjusted to null their excitation profile in the carbonyl region. Band-selective excitation and inversion of aliphatic carbon spins was accomplished by Gaussian cascades G4 and G3 (Emsley and Bodenhausen, 1990), respectively, with every other G4 pulse having a time-reversed shape. Durations are (A) 0.5 ms, G3; (B): 1.3 ms, G3; 1.8 ms, G4; and (C) 0.3 ms, first G3; 0.5 ms, second G3; 0.5 ms, G4. The G3 pulse applied during the t_1 constant-time evolution period in C is centred at 45.4 ppm by phase modulation. Carbonyl 90° and 180° pulses are sinc-shaped and have a constant duration of 124 μs while differing in amplitude. z-Gradient pulses G_1, G_2 and G_3 are sine-bell shaped with typical durations and approximate centre amplitudes of 1 ms/10 G cm^{-1}, 1 ms/5 G cm^{-1} and 0.8 ms/35 G cm^{-1}, respectively. Delays are adjusted as follows: $\tau = 2.3$ ms, $\eta = 5.4$ ms, $\delta = 28.5$ ms, $\tau' = 2.7$ ms. In scheme C, the constant-time period T is set to 27.4 ms. Phase cycles are (A): ϕ_1 = y,–y, ϕ_2 = 2(x),2(–x), ϕ_3 = y, ϕ_4 = –y, ϕ_5 = 8(x),8(–x), ϕ_6 = x + 25°, ϕ_7 = 4(x),4(–x), ϕ_8 = 8(x),8(y), ϕ_9 = x + 47°, ϕ_{10} = –x, rec. = x,2(–x),x,–x,2(x),–x; (B) ϕ_1 = y,–y, ϕ_2 = 2(x),2(–x), ϕ_3 = y, ϕ_4 = –y, ϕ_5 = 4(x),4(–x), ϕ_6 = x + 25°, ϕ_7 = 8(x),8(–x), ϕ_8 = x – 18°, ϕ_9 = –x, rec. = x,2(–x),x,–x,2(x),2(–x),2(x),–x,x,2(–x),x; and (C) ϕ_1 = y,–y, ϕ_2 = 2(x),2(–x), ϕ_3 = y, ϕ_4 = –y, ϕ_5 = 4(x),4(–x), ϕ_6 = x + 7°, ϕ_7 = 8(x),8(–x), ϕ_8 = x – 45°, ϕ_9 = –x, rec. = x,2(–x),x,–x,2(x),2(–x),2(x),–x,x,2(–x),x. States-TPPI type (Marion et al., 1989b) quadrature detection in the t_1 and t_2 dimensions involves incrementing phases ϕ_5 and ϕ_7, respectively. Phases ϕ_6 and ϕ_9 in sequence A and ϕ_6 and ϕ_8 in sequences B and C are adjusted to compensate for zero-order Bloch–Siegert phase errors, as indicated.

we will focus on vicinal couplings related to the backbone torsion angle ϕ, which is characterized by three ^{1}H,^{13}C, a single ^{1}H,^{1}H and two ^{13}C,^{13}C three-bond couplings. Usually, a reduced set made up of the homonuclear $^3J(H^N,H^{\alpha})$ interaction and the heteronuclear coupling constants $^3J(H_i^N,C_i')$, $^3J(H_i^N,C_i^{\beta})$ and $^3J(C'_{i-1},H_i^{\alpha})$, which were all parametrized by Wang and Bax (1995,1996) using human ubiquitin as a model protein, serves as the experimental basis. In contrast, the circumjacent carbon–carbon couplings have only very recently been addressed (Hu and Bax, 1996a,b; Löhr and Rüterjans, 1996), although approximate values for $^3J(C'_{i-1},C_i^{\beta})$ in alanine residues in calmodulin

were reported previously (Grzesiek et al., 1993). The purpose of the present work is twofold. Firstly, accurate carbonyl-related coupling constants $^3J(C'_{i-1},H_i^\alpha)$, $^3J(C'_{i-1},C_i^\beta)$ and $^3J(C'_{i-1},C'_i)$ are measured using a family of triple-resonance E.COSY-type experiments. Secondly, empirical Karplus parameters associated with these coupling constants are proposed for use in protein structure determination.

The new methods are applied to the protein flavodoxin originating from the sulphate-reducing organism *Desulfovibrio vulgaris*. It consists of 147 amino acid residues and a non-covalently yet very tightly bound flavin mononucleotide (FMN) as the redox-active cofactor. The tertiary structure of the protein in its three redox states is well characterized by X-ray crystallography (Watenpaugh et al., 1972,1973; Watt et al., 1991). Recent NMR investigations of oxidized flavodoxin revealed that the ϕ,ψ backbone fold in solution mainly conforms with the crystal structure (Stockman et al., 1994; Knauf et al., 1996). The experimental $^3J(C'_{i-1},H_i^\alpha)$, $^3J(C'_{i-1},C_i^\beta)$ and $^3J(C'_{i-1},C'_i)$ coupling constants allow parametrizing the respective Karplus relations on the basis of ϕ-angles derived from the X-ray structure of *Desulfovibrio vulgaris* flavodoxin at 1.7 Å resolution (M. Walsh (1996) unpublished results).

Materials and Methods

NMR measurements

Recently we applied a novel three-dimensional E.COSY-based method which can be adapted for the measurement of either $^3J(C'_{i-1},H_i^\alpha)$, $^3J(C'_{i-1},C_i^\beta)$ or $^3J(C'_{i-1},C'_i)$ coupling constants (Löhr and Rüterjans, 1996). The respective pulse sequences are of the 'out-and-back' type involving initial excitation as well as final detection of amide proton spins. As a drawback, the signal intensity is diminished by the dephasing of water magnetization if these amide sites are subject to fast proton exchange with the solvent. Here, we present improved pulse schemes, in which the undesired saturation transfer is avoided by maintaining control of the water magnetization vector throughout the sequences.

The three pulse sequences that were used to determine $^3J(C'_{i-1},H_i^\alpha)$, $^3J(C'_{i-1},C_i^\beta)$ and $^3J(C'_{i-1},C'_i)$ coupling constants are depicted in Fig. 1. They rely on a common coherence-transfer mechanism, but differ in the type of passive spin ($^1H^\alpha$, $^{13}C^\beta$ or $^{13}C'$) involved in generating the E.COSY multiplet patterns (Griesinger et al., 1985,1986,1987). The magnetization transfer pathway employed was inspired by a dimensionality-reduced sequence termed COHNNCA particularly designed for the simultaneous detection of both $^{13}C_i^\alpha$ and $^{13}C'_{i-1}$ in a single frequency dimension (Szyperski et al., 1995). Following the initial ^1H-^{15}N polarization transfer, nitrogen magnetization spreads out on both adjacent carbon nuclei, i.e. $^{13}C^\alpha$ and $^{13}C'$ of the same and the preceding amino acid residue, respectively. This is achieved by a simultaneous build-up of ^{15}N antiphase magnetization with respect to either species during the delay period δ. The chemical shifts of the α and carbonyl carbons are then sampled consecutively without any further transfer step. Finally, the magnetization is relayed via the nitrogen spin back to the amide proton for detection. We refer to the E.COSY-type experiments presented here as H(N)CA,CO, where the comma indicates that a simultaneous $N \rightarrow C^\alpha$, $N \rightarrow C'$ rather than a sequential $N \rightarrow C^\alpha \rightarrow C'$ transfer takes place.

In pulse scheme A of Fig. 1, the DIPSI-2 decoupling sequence on protons is gated off during t_1 and t_2. As a consequence, cross peaks are split in the $^{13}C^\alpha$ dimension by the large $^1J(C^\alpha,H^\alpha)$ coupling. Preserving the state of the passive $^1H^\alpha$ spin between durations t_1 and t_2 leads to a displacement of the multiplet components along the $^{13}C'$ axis due to $^{13}C',^1H^\alpha$ scalar interactions, which enables the magnitude of the long-range coupling constants to be accurately determined. Vicinal and geminal $^{13}C',^1H^\alpha$ coupling constants are obtained from E.COSY multiplets arising from magnetization transfer via $^1J(N,C^\alpha)$ and $^2J(N,C^\alpha)$, respectively. The sensitivity of the H(N)CA,CO experiment is comparable to that of a ct-HNCA (Grzesiek and Bax, 1992), although the splitting by the one-bond coupling in t_1 reduces the signal-to-noise ratio by a factor of 2. The measuring time required might therefore be mainly controlled by the resolution in the indirectly detected carbonyl dimension. In such cases, either signal aliasing or chemical-shift scaling (Hosur et al., 1985; Krishnamurthy, 1995) can be applied to reduce the number of time-domain data points without degrading the accuracy of the frequency determination of the individual E.COSY multiplet components. The second alternative is employed in the $^1H^\alpha$-coupled H(N)CA,CO sequence (Fig. 1A). A pair of 180° pulses applied to proton and carbonyl-carbon spins is shifted from the centre of the t_2 evolution period at half the incrementation rate. Thus, the splittings due to $^{13}C',^1H^\alpha$ couplings are scaled up twofold with respect to carbonyl chemical shifts and the desired time-domain resolution is afforded with half the number of t_2 increments. Inversion pulses on ^{15}N and $^{13}C^\alpha$ nuclei are displaced from the 180° $^{13}C'$ pulse by $t_2/2$ to refocus $^1J(N,C')$ and $^1J(C^\alpha,C')$ interactions. Note that arbitrary values of the scaling factor can in principle be chosen according to the intended duration of the experiment.

$^3J(C'_{i-1},C_i^\beta)$ coupling constants were measured using the pulse sequence of Fig. 1B. While proton spins are decoupled during t_1, the homonuclear $^1J(C^\alpha,C^\beta)$ interaction leads to a splitting in the $^{13}C^\alpha$ domain, provided the evolution time is sufficiently long. Perturbation of $^{13}C^\beta$ spin states is avoided by employing G3 and G4 Gaussian cascades (Emsley and Bodenhausen, 1990) for band-selective inversion and excitation of $^{13}C^\alpha$ magnetization, respectively. The pulse widths were adjusted to obtain a uniform excitation profile limited to the region between 50 and 68 ppm to avoid affecting carbon resonances

upfield from ≈43 ppm. These precautions allow the evaluation of E.COSY cross peaks for all the amino acids except for serine and threonine, whose $^{13}C^{\alpha}$ and $^{13}C^{\beta}$ resonance regions usually overlap.

$^{3}J(C'_{i-1},C'_{i})$ coupling constants are determined using $^{1}J(C^{\alpha},C')$ as the associated coupling. In order to resolve this one-bond splitting, it is necessary to remove the effect of the coupling between α- and β-carbons. Therefore, in the pulse scheme shown in Fig. 1C, the $^{13}C^{\alpha}$ evolution period is implemented in a constant-time manner with T adjusted to $1/^{1}J(C^{\alpha},C^{\beta})$. As the coupling to be determined is homonuclear, a small-flip-angle mixing pulse on the carbonyl spins at the beginning of the t_2 evolution period warrants the E.COSY-like multiplet pattern by restricting coherence transfer to directly connected transitions (Griesinger et al., 1986). Cross peak patterns provided by each of the three versions of the H(N)CA,CO-E.COSY experiment are depicted schematically in Fig. 2.

Solvent suppression in the H(N)CA,CO pulse sequences is accomplished by the WATERGATE technique (Piotto et al., 1992) implemented during the final reverse INEPT transfer. Although no pre-irradiation on the water signal is thus required, the signal intensity of fast-exchanging amide protons is usually reduced due to saturation transfer caused by the dephased water magnetization (Li and Montelione, 1993). This effect can, however, be avoided by keeping the water magnetization vector along the z-axis during the application of pulsed-field gradients (Grzesiek and Bax, 1993a,b; Stonehouse et al., 1994). In order to improve our original pulse schemes (Löhr and Rüterjans, 1996,1997), additional water-selective flip-back pulses are applied with phases +x and −x immediately following the initial 2τ period and prior to the final 90° ^{1}H hard pulse, respectively, to restore H_2O magnetization along +z. The 180° non-selective proton pulse between t_2 and the second DIPSI-2 period compensates the effect of the inversion pulse applied during t_2. Furthermore, it is critical to protect the solvent magnetization from rf inhomogeneity effects, caused by the proton composite-pulse decoupling sequence. The magnetization is temporarily aligned with the DIPSI-2 spin-lock axis and subsequently returned to +z (Kay et al., 1994). These 90° (y/−y) pulses have no deteriorating effect on amide protons, the ^{15}N antiphase magnetization with respect to directly bound protons just being completely refocused.

All experiments were carried out at 27 °C using a Bruker DMX 600 spectrometer. The instrument was equipped with a 5 mm $^{1}H\{^{13}C,^{15}N\}$ triple-resonance probe with actively shielded x, y and z gradient coils and pulsed-field gradient accessories. Spectra were recorded on a 1.4 mM sample of uniformly $^{13}C/^{15}N$-labelled *Desulfovibrio vulgaris* flavodoxin dissolved in 95% H_2O/5% D_2O containing 10 mM potassium phosphate (pH = 7.0) and trace amounts of sodium azide. The spectral width in the F2 ($^{13}C'$) dimension was uniquely 1087 Hz in the three versions of the H(N)CA,CO pulse sequence. In F3 ($^{1}H^{N}$) spectral widths were set to 9615 Hz in versions A and C and to 7184 Hz in version B, while in F1 ($^{13}C^{\alpha}$) they comprised 3125, 1326 and 2336 Hz in versions A, B and C, respectively. Note that in version A, the spectral width in F2 refers to the evolution of chemical shifts such that t_2 is incremented at twice the rate employed in the other experiments. The number of complex data points recorded (and the corresponding acquisition times in parentheses) in F1, F2 and F3, respectively, were (A) 44 (14.1 ms), 52 (95.6 ms), 1024 (106.5 ms), (B) 60 (45.2 ms), 86 (79.2 ms), 768 (107 ms) and (C) 64 (27.2 ms), 86 (79.2 ms), 1024 (106.5 ms). Each of the H(N)CA,CO experiments was executed twice, differing solely in the scan repetition rate. The total accumulation times were 39 + 42 h, 89.5 + 92 h and 88 + 95 h for versions A, B and C, respectively, using 16 scans per FID in each case.

In addition, a $^{13}C'$-coupled (H)NCAHA experiment (Löhr and Rüterjans, 1995) was performed in order to measure $^{3}J(C'_{i-1},H^{\alpha}_{i})$ coupling constants. The sequence was modified to incorporate gradient-coherence selection in the final polarization transfer (Boyd et al., 1992; Davis et al., 1992). Acquisition times were 88.3, 15.4 and 111.5 ms in the t_1 (^{15}N), t_2 ($^{13}C^{\alpha}$) and t_3 ($^{1}H^{\alpha}$) domains, respectively. Sixteen scans were recorded per FID, leading to a measuring time of 82 h.

Processing and evaluation of spectra

Data sets were processed and displayed on SGI workstations using the FELIX 1.1 program (Hare Research Inc., Woodinville, WA, U.S.A.). The residual H_2O signal was eliminated by convolution of the time-domain data along t_3 (Marion et al., 1989a). In order to obtain phase sensitivity in the (H)NCAHA spectrum, FIDs selected for echo and antiecho coherence-transfer pathways were combined as described by Nagayama (1986). The semi-constant-time ^{15}N dimension of the $^{13}C'$-coupled (H)NCAHA was resolution-enhanced by one-third using conventional linear prediction. Mirror-image linear prediction (Zhu and Bax, 1990) was employed to extend the $^{13}C^{\alpha}$ time-domain data of both the $^{13}C'$-coupled H(N)CA,CO (Fig. 1C) and (H)NCAHA experiments by approximately 40% of their original size. Prior to Fourier transformation, data were multiplied with a squared-cosine function in all dimensions except for the t_1 ($^{13}C^{\alpha}$) domain of the $^{13}C^{\beta}$-coupled H(N)CA,CO (Fig. 1B) and the t_1 (^{15}N) domain of the $^{13}C'$-coupled (H)NCAHA, where apodization involved squared sine-bell functions shifted by π/5 and π/3, respectively. The initial evolution time t_2 was adjusted to $[SW(^{13}C')]^{-1}$ in all H(N)CA,CO experiments. During processing, t_2 data were prefixed by a linearly backward predicted sampling point in order to circumvent any zero- and first-order phase corrections.

Vicinal coupling constants were extracted from the E.COSY-type multiplets by a trace-alignment procedure.

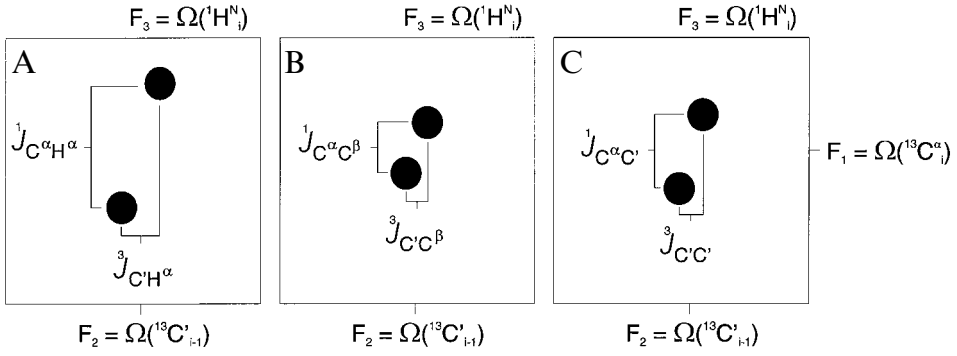

Fig. 2. Schematic representation of the cross peaks obtained with each of the H(N)CA,CO pulse sequences depicted in Fig. 1. Only the intraresidual correlations (i.e. those at F1 = $\Omega(C_i^{\alpha})$, F3 = $\Omega(H_i^{N})$) are shown. E.COSY-type patterns arise in the planes perpendicular to the acquisition dimension. The desired vicinal coupling constants are taken from the F2 displacement of the two major multiplet components separated by one-bond couplings in F1.

In H(N)CA,CO spectra, two F2 traces corresponding to upper and lower E.COSY multiplet components were generated by summing over appropriate spectral points in F1 and F3. In an analogous way, F3 traces were obtained from (H)NCAHA multiplets. After zero-filling and Fourier transformation, the digital resolution was 4.24 Hz in the F2 ($^{13}C'$) domain of the H(N)CA,CO spectra and 4.48 Hz in the F3 ($^{1}H^{\alpha}$) domain of the (H)NCAHA data set. In order to avoid the limited accuracy imposed by the sampling grid in the frequency domain, the traces were inversely Fourier transformed and subjected to a least-squares superposition in the time domain (Schmidt et al., 1995).

Calculation of Karplus coefficients

Data were fitted to the expression $^{3}J(\theta_i) = A_k \cos^2\theta_i + B_k \cos\theta_i + C_k$, where the index i runs over the individual amino acid residues for which the respective coupling constants could be measured. Solving the overdetermined system of linear equations using Gaussian elimination and QR decomposition with pivoting (Press et al., 1989) yielded the desired Karplus parameters. Reference ϕ dihedral angles were derived from the 1.7 Å X-ray structure of oxidized *Desulfovibrio vulgaris* flavodoxin (M. Walsh (1996) unpublished results), assuming ideal tetrahedral and planar geometry at the α-carbon and nitrogen sites, respectively, i.e. $\theta(C'_{i-1},H_i^{\alpha}) = \phi + 120°$, $\theta(C'_{i-1},C_i^{\beta}) = \phi - 120°$ and $\theta(C'_{i-1},C'_i) = \phi$. For glycine residues, the identities hold when $H_i^{\alpha 2}$ and $H_i^{\alpha 3}$ are substituted for H_i^{α} and C_i^{β}, respectively. To assess the uncertainty of the coefficients A, B and C, each of the fits was repeated 10 000 times while randomly omitting approximately 10% of the ^{3}J-values measured (Vuister and Bax, 1993).

Results

Experimental carbonyl-related J coupling constants in flavodoxin

The three interresidual vicinal couplings related to the ϕ dihedral angle have been investigated in flavodoxin using the H(N)CA,CO-E.COSY method. Figure 3 presents examples for the multiplet patterns obtained with each pulse-sequence variant. The peaks exhibit a larger splitting along the F1 ($^{13}C^{\alpha}$) axis due to one-bond couplings and a smaller displacement in the F2 ($^{13}C'$) domain which provides a measure for the ^{3}J interaction. It is apparent from the traces through the upper and the lower F1 doublet components that the optimal superposition does not depend on the digital resolution in F2 as the alignments were carried out in the t_2 time domain. A total of 86 $^{3}J(C'_{i-1},H_i^{\alpha})$, 101 $^{3}J(C'_{i-1},C_i^{\beta})$ and 121 $^{3}J(C'_{i-1},C'_i)$ values could thus be extracted. To estimate the experimental reproducibility of the measurements, each experiment was repeated after several weeks. Mainly identical pulse sequences were used, except for slightly longer/shorter preparation delays and readjusted shim and pulse-power levels. The pairwise rms differences in the J-values were 0.37, 0.38 and 0.55 Hz, indicating random errors in the mean J-values of 0.19 Hz for $^{3}J(C'_{i-1},H_i^{\alpha})$ and $^{3}J(C'_{i-1},C_i^{\beta})$ and 0.28 Hz for $^{3}J(C'_{i-1},C'_i)$.

For glycine residues, the $^{1}J(C^{\alpha},H^{\alpha})$ interactions lead to a triplet multiplicity in the F1 dimension of the $^{1}H^{\alpha}$-coupled H(N)CA,CO, preventing a separate determination of the two $^{3}J(C'_{i-1},H_i^{\alpha})$ coupling constants. The desired data were alternatively obtained by an (H)NCAHA-E.COSY experiment which exploits $^{1}J(C'_{i-1},N_i)$ as the associated passive coupling and allows extracting $^{3}J(C'_{i-1},H_i^{\alpha 2})$ and $^{3}J(C'_{i-1},H_i^{\alpha 3})$ from distinct F1,F3 multiplets (Löhr and Rüterjans, 1995). Unambiguous $H^{\alpha 2}/H^{\alpha 3}$ stereospecific assignments on the basis of NOE–distance relationships were possible for eight out of 18 glycine residues in flavodoxin and only these pairs of coupling constants were included in the subsequent Karplus parametrization. Representative examples are shown in Fig. 4. The signal-to-noise ratio of these signals was significantly poorer than that of H(N)CA,CO signals, implying a reduced precision for the glycine $^{3}J(C'_{i-1},H_i^{\alpha})$ coupling constants. The (H)NCAHA-E.COSY experiment yielded additional

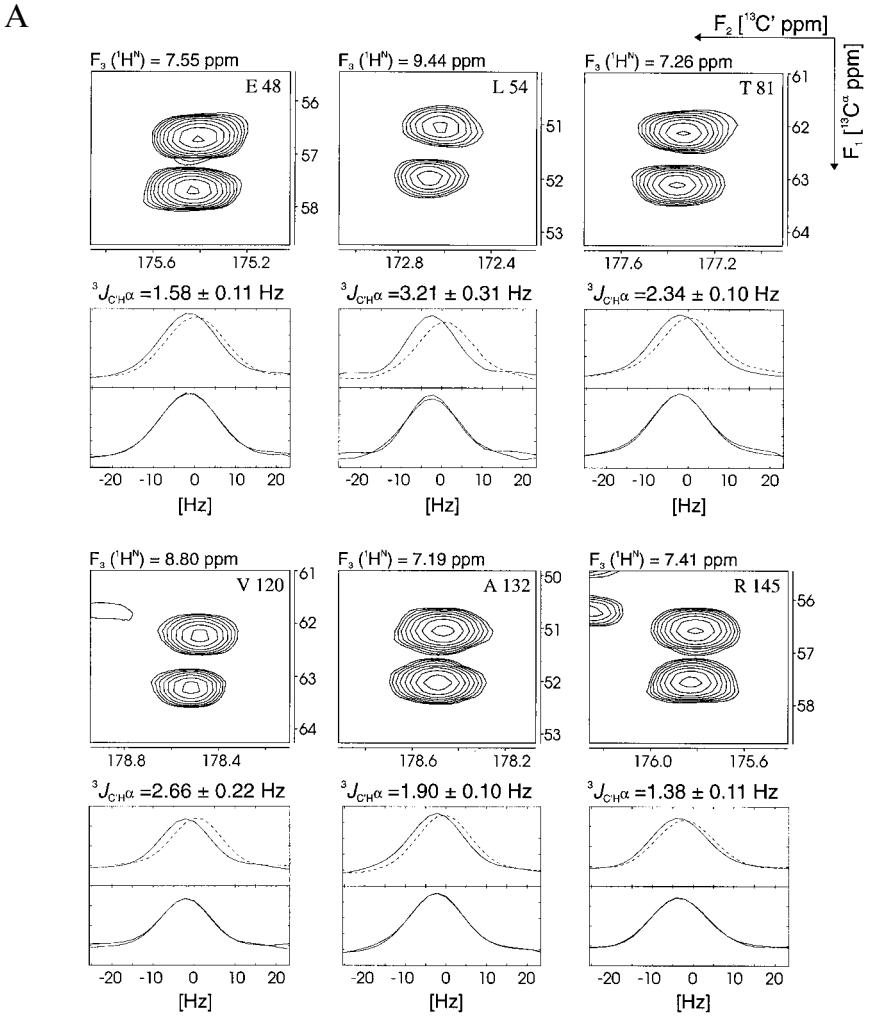

Fig. 3. Extraction of (A) $^3J(C'_{i-1},H_i^{\alpha})$, (B) $^3J(C'_{i-1},C_i^{\beta})$ and (C) $^3J(C'_{i-1},C'_i)$ coupling constants from cross peaks in 3D H(N)CA,CO-E.COSY spectra of flavodoxin. The upper half of each panel shows expansions of F1/F2 slices which contain the intraresidual cross peaks of the amino acid indicated. In all plots the level-spacing multiplier is uniformly set to $2^{1/2}$. Note that in part A both $^3J(C'_{i-1},H_i^{\alpha})$ splittings and $^{13}C'$ line widths are scaled up by a factor of 2 relative to the F2 chemical-shift axis. One-dimensional projections of the high-field (dashed line) and low-field (solid line) multiplet halves are obtained by summing over appropriate spectral points in F1 and F3. A superposition of the fitted traces is shown at the bottom of each panel. The resulting values for the vicinal coupling constants are indicated. The cross peak for Gly^{116} in part C is folded in the F1 dimension. Its negative intensity is due to the lack of a homonuclear coupling partner during the $^{13}C^{\alpha}$ constant-time evolution period in the pulse sequence of Fig. 1C. In contrast, cross peaks in part B that are folded in F1 are negative because of a 180° first-order phase correction along this dimension. The weak cross peak in the panel of Ala^{39} is the sequential correlation to Ala^{38} $^{13}C^{\alpha}$ from which a geminal C'_{i-1},C_{i-1}^{β} coupling of -2.26 ± 0.34 Hz can be determined. Arg^{86} follows a glycine residue in the amino acid sequence of flavodoxin, leading to a partial splitting of the cross peak in the $^{13}C'$ domain, as explained in the text.

$^3J(C'_{i-1},H_i^{\alpha})$ coupling constants of 30 non-glycine residues for which a multiplet evaluation in the $^1H^{\alpha}$-coupled H(N)CA,CO spectrum was impeded due to signal overlap. Among the three H(N)CA,CO experiments, the $^1H^{\alpha}$-coupled version (Fig. 1A) is most prone to overlap because of both the space-consuming splitting in F1 and the upscaling of line widths and couplings with respect to chemical shifts in F2. If the sensitivity of the experiment becomes critical because of low sample concentrations, it is advisable to prolong the measuring time by abandoning chemical-shift scaling to increase the spectral resolution rather than by doubling the number of scans (Löhr and Rüterjans, 1997).

Dihedral-angle dependence of the carbonyl-related couplings

The total number of $^3J(C'_{i-1},H_i^{\alpha})$ couplings used for the Karplus parametrization was 132. In Fig. 5A, these values are plotted versus the ϕ torsion angles derived from the flavodoxin X-ray structure together with the optimized Karplus curve which is represented by

$$^3J(C'_{i-1},H_i^{\alpha}) = 3.72\ \cos^2(\phi + 120°) - 1.71\ \cos(\phi + 120°) + 1.07 \quad (2)$$

The residual violation between predicted and experimental ^3J coupling constants is 0.41 Hz. Although equally weighted, data points obtained for glycine resi-

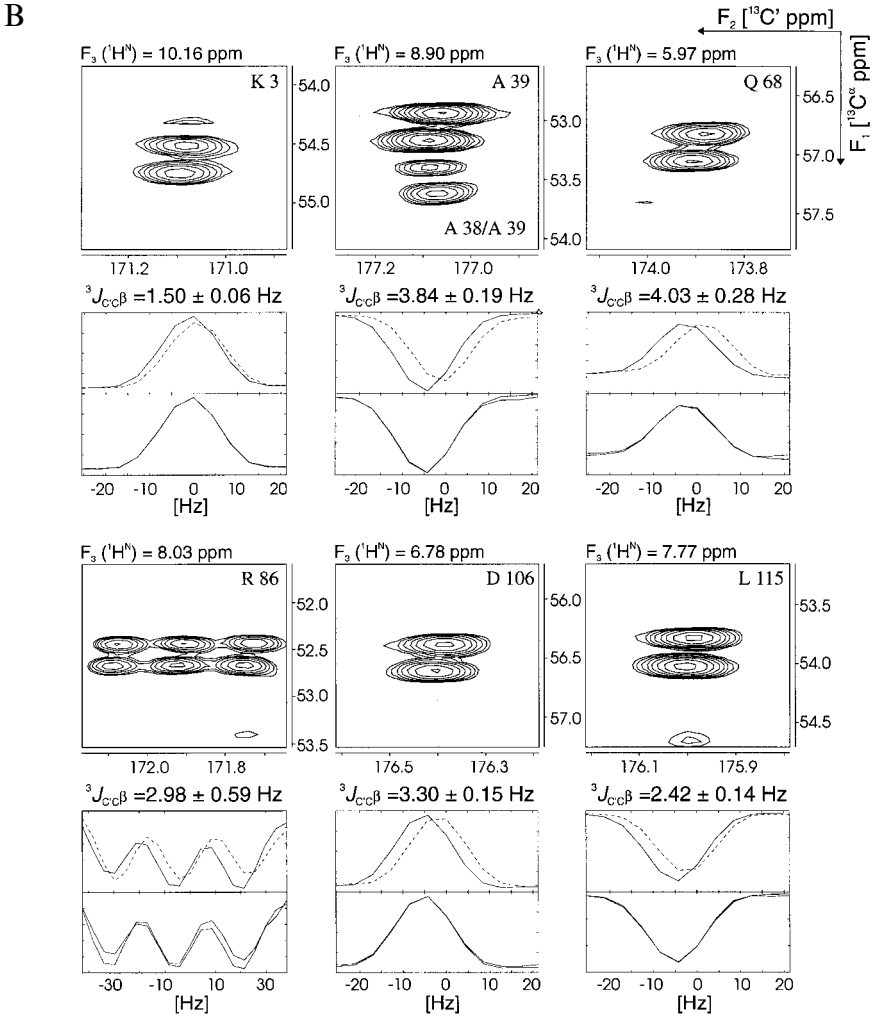

Fig. 3. (continued).

dues are marked differently in Fig. 5A as their experimental precision is lower compared to other calibration points.

The experimental determination of $^3J(C'_{i-1},C_i^\beta)$ coupling constants is shown in Fig. 3B. The comparatively small $^1J(C^\alpha,C^\beta)$ splitting in F1 gives rise to a less extent of intra- and interresidual multiplets and reduces overlap to only a few cases. In the F2 dimension only partial refocusing of the $^1J(C^\alpha,C')$ interaction due to imperfect inversion of glycine α-carbon spins, which resonate upfield from the $^{13}C^\alpha$ region of the remaining residues, is achieved because the 180° pulse in the centre of t_2 is designed not to affect $^{13}C^\beta$ spin states. As a consequence, the E.COSY F1,F3 multiplets at the $^{13}C^\alpha/^1H^N$ position of amino acids preceded by glycine are 'pseudo' triplets along F2, exhibiting a splitting of approximately 55 Hz for the two outer lines (e.g. Arg[86] in Fig. 3B). Excluding the glycine, proline, serine and threonine residues, C'_{i-1},C_i^β vicinal couplings were quantitatively measured for 101 out of 111 potential amino acids. Values ranging between 0.15 and 4.15 Hz were used in the parametrization of the Karplus equation, yielding

$$^3J(C'_{i-1},C_i^\beta) = 2.54\cos^2(\phi - 120°) - 0.55\cos(\phi - 120°) + 0.37 \quad (3)$$

a graphical representation of which is given in Fig. 5B. The rmsd between coupling constants measured and the values predicted from the X-ray ϕ dihedral angles amounts to 0.33 Hz.

The smallest coupling constants and actually the only negative values have been measured for the homonuclear $^{13}C',^{13}C'$ interaction. The correlation between these vicinal couplings and the intervening torsional angle in the crystal structure is shown in Fig. 5C. The optimized Karplus curve given by

$$^3J(C'_{i-1},C'_i) = 1.57\cos^2\phi - 1.07\cos\phi + 0.49 \quad (4)$$

with an rms deviation of 0.32 Hz from the experimental J-values indicates an almost vanishing coupling in the vicinity of $\phi = \pm 70°$ but does not undergo a sign change.

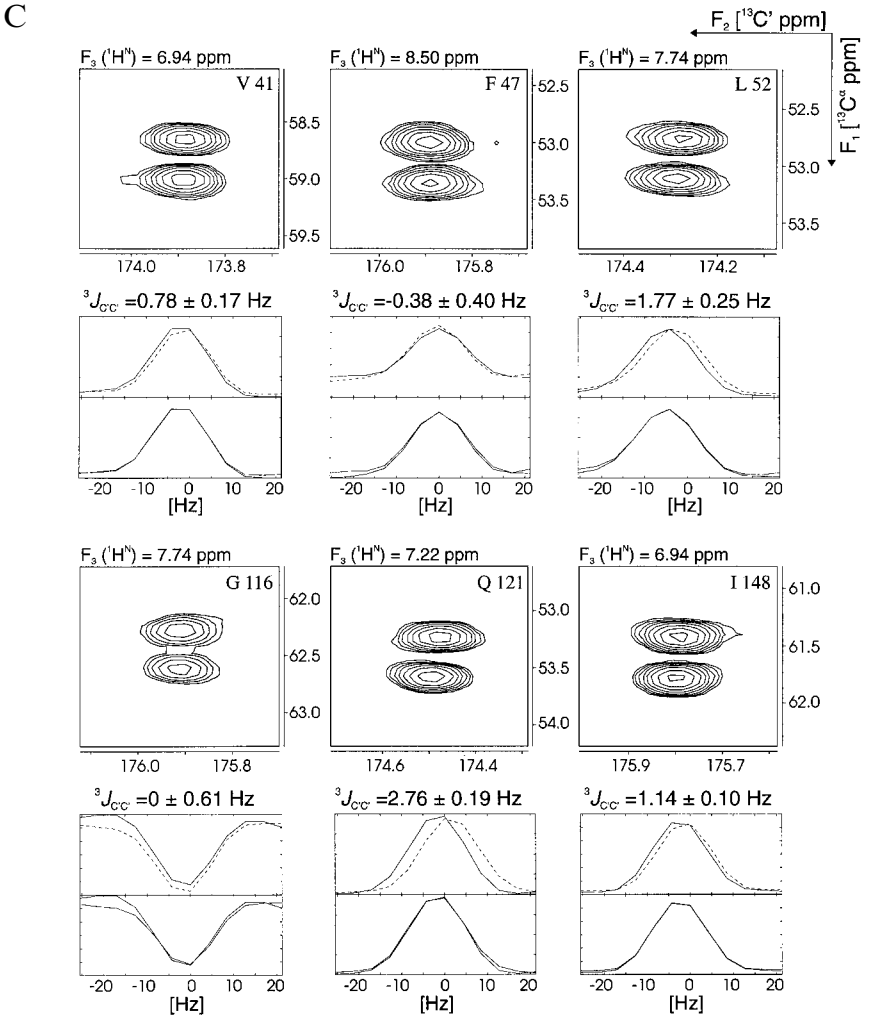

Fig. 3. (continued).

Discussion

In Fig. 6, the results of our study are compared with previously published Karplus curves, and a comparison of the coefficients in Eqs. 2–4 with very early parametrizations reveals marked differences. Disregarding theoretical approaches, parametrizations of $^3J(C'_{i-1},H_i^{\alpha})$ based on experimental data were selected for comparison. Parametrization of the dihedral-angle dependence of the $^3J(C'_{i-1},H_i^{\alpha})$ coupling by Bystrov et al. (1975) exploits conformationally averaged ^{3}J-values of amino acid derivatives combined with the coupling determined for a fixed dihedral angle of 90°. Vicinal ^{13}C(O)-N-C-^{1}H coupling constants were measured for lactam and amide fragments of defined geometry, mimicking the protein backbone (Kao and Barfield, 1985). Interestingly, the $^3J(C'_{i-1},H_i^{\alpha})$ Karplus curve that results from our protein data, while suggesting the maximum of $^3J(C'_{i-1},H_i^{\alpha})$ at $\phi = +60°$ to be lower by more than 5 Hz compared to the Bystrov curve, almost coincides with that given by Kao and Barfield (1985), although the latter is based on J coupling constants measured in small organic compounds. In contrast, their coefficients empirically determined for the vicinal couplings between carbonyl and aliphatic carbons across amide linkages in the same molecules deviate significantly from our $^3J(C'_{i-1},C_i^{\beta})$ parametrization. Experimental ^{3}J carbon–carbon couplings were found to be generally larger than predicted by FPT-INDO calculations (Solkan and Bystrov, 1974).

Significant similarity is found when our results are compared to those of Bax and co-workers, who recently correlated the coupling constants measured for human ubiquitin with the ϕ-angles from its crystal structure (Hu and Bax, 1996a,b; Wang and Bax, 1996). However, in the negative torsion-angle range, both the $^3J(C'_{i-1},H_i^{\alpha})$ and $^3J(C'_{i-1},C'_i)$ coupling constants measured in flavodoxin vary stronger with ϕ than those determined in ubiquitin, resulting in intersections of the respective curves.

The H(N)CA,CO-E.COSY concept applied to isotopically enriched polypeptides turned out to be a versatile method for the determination of vicinal couplings between backbone carbonyl ^{13}C nuclei and $^1H^{\alpha}$, $^{13}C^{\beta}$ or ^{13}C' spins of the following residue. While the extraction of ^{13}C,^{13}C

coupling constants from an indirectly detected spectrum dimension is mandatory for sensitivity reasons, it is optional in the case of $^3J(C'_{i-1},H_i^\alpha)$. Several advantages render the H(N)CA,CO scheme superior for the measurement of the latter coupling, too. Firstly, the magnetization transfer is more efficient than in $^{13}C'$-coupled (H)NCAHA (Löhr and Rüterjans, 1995) and HCAN[C']-E.COSY (Wang and Bax, 1996) experiments which include periods with durations of $1/^1J(C^\alpha,C^\beta)$ and $2/^1J(C^\alpha,C^\beta)$, respectively, during which the rapid transverse relaxation of $^{13}C^\alpha$ nuclei can take place. Secondly, sensitivity gains compared to E.COSY schemes in which the coupling of interest occurs along a $^1H^\alpha$ domain result from the fact that the $^{13}C'$ resonances are considerably less broadened by unresolved homonuclear couplings. Thirdly, the long transverse relaxation time of $^{13}C'$ compared to that of $^1H^\alpha$ warrants higher resolution and thus a more precise determination of the vicinal coupling constants. Finally, the detection of amide ^1H instead of α-proton resonances during acquisition avoids interference of the abundant solvent signal with the quantitative cross-peak evaluation. This problem is circumvented in the HCAN[C']-E.COSY method as it is possible to conduct the experiment on a protein sample dissolved in D_2O. In the (H)NCAHA experiment carried out in this study, however, although good water suppression was achieved using gradient-coherence selection, $^3J(C'_{i-1},H_i^\alpha)$ coupling constants could not be reliably measured for residues with $^1H^\alpha$ spins resonating within ±0.15 ppm of the H_2O signal. Therefore, $^3J(C'_{i-1},H_i^\alpha)$ values emerging from the $^{13}C'$-coupled (H)NCAHA spectrum were used in the parametrization only when spectral overlap impeded their analysis in the H(N)CA,CO-E.COSY.

In proteins, the measurement of vicinal coupling constants involving α-protons is hampered by differential relaxation of in-phase and antiphase coherences caused by a rapid $^1H^\alpha$ spin flip rate (Harbison, 1993; Norwood, 1993; Norwood and Jones, 1993). Therefore, one might expect that the accuracy of $^3J(C'_{i-1},H_i^\alpha)$ values measured in an H(N)CA,CO-E.COSY experiment which assigns $^1H^\alpha$ the role of a passive spin is inferior compared to the data from HCAN[C']- or (H)NCAHA-E.COSY pulse schemes which finally detect transverse $^1H^\alpha$ magnetization, leaving carbonyl spins unperturbed throughout the sequences. However, the simultaneous build-up of ^{15}N antiphase magnetization with respect to both α and carbonyl carbons in the H(N)CA,CO allows an immediate succession of the two ^{13}C chemical shift evolution periods with a vanishing time in which $^1H^\alpha$ spin flips can take place. In fact, for those residues, where $^3J(C'_{i-1},H_i^\alpha)$ coupling constants were obtained with both methods employed here, no systematic deviation towards lower values in the H(N)CA,CO was observed.

As a drawback of the H(N)CA,CO-E.COSY method, $^3J(C'_{i-1},H_i^\alpha)$ coupling constants cannot be measured for glycine spin topologies. Since the absolute maximum of the respective Karplus curve falls in the positive ϕ-angle range and flavodoxin contains only two non-glycine residues with positive ϕ-angles, it was critical to supplement the data set with glycine $^3J(C'_{i-1},H_i^\alpha)$ coupling constants obtained in the $^{13}C'$-coupled (H)NCAHA. Each of the eight glycine residues that allowed a determination of the couplings provided one calibration point in the +ϕ range, either for the α2 or the α3 proton. As already discussed,

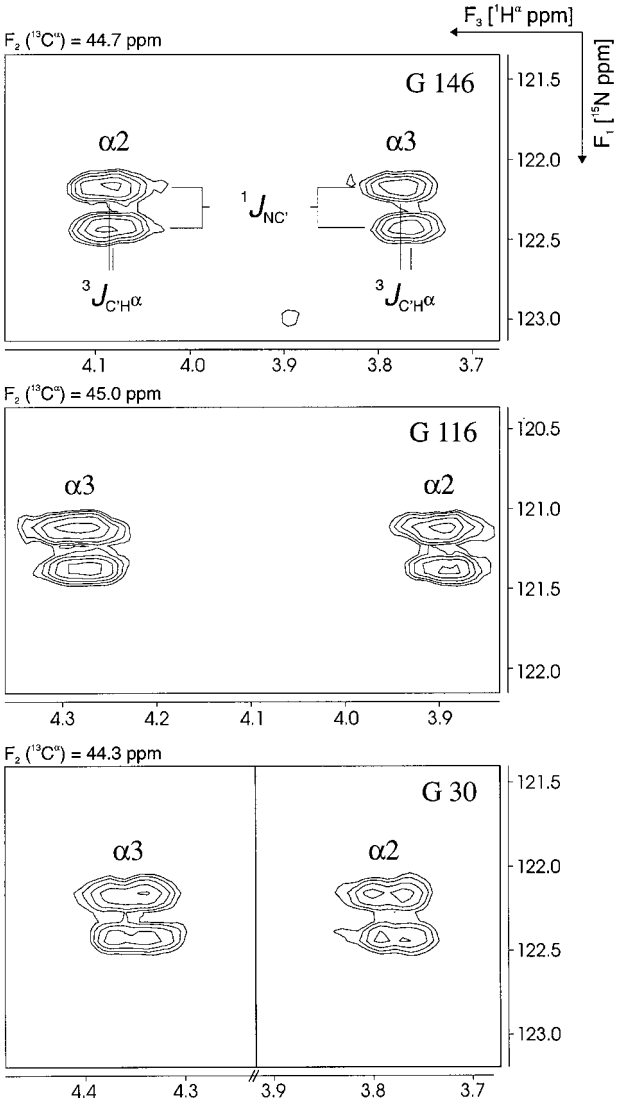

Fig. 4. Determination of glycine $^3J(C'_{i-1},H_i^\alpha)$ coupling constants in F1/F3 slices from a $^{13}C'$-coupled (H)NCAHA spectrum of *Desulfovibrio vulgaris* flavodoxin. The same level-spacing multiplier as in Fig. 3 (i.e. $2^{1/2}$) is employed. Signals are folded in the F1 (^{15}N) dimension such that their true chemical-shift values are smaller by 14.7 ppm. Stereospecific assignments of the prochiral proton resonances are marked. In the upper panel, the scalar interactions relevant for the E.COSY multiplet pattern are indicated. The values measured are $^3J(C'_{i-1},H_i^{\alpha 2}) = 1.76 \pm 1.16$ Hz, $^3J(C'_{i-1},H_i^{\alpha 3}) = 5.20 \pm 0.54$ Hz (Gly^{146}), $^3J(C'_{i-1},H_i^{\alpha 2}) = 5.08 \pm 0.94$ Hz, $^3J(C'_{i-1},H_i^{\alpha 3}) = 3.32 \pm 1.18$ Hz (Gly^{116}) and $^3J(C'_{i-1},H_i^{\alpha 2}) = 4.36 \pm 1.34$ Hz, $^3J(C'_{i-1},H_i^{\alpha 3}) = 2.42 \pm 0.93$ Hz (Gly^{30}). The large standard deviations compared to evaluations from H(N)CA,CO spectra reflect the lower signal-to-noise ratio.

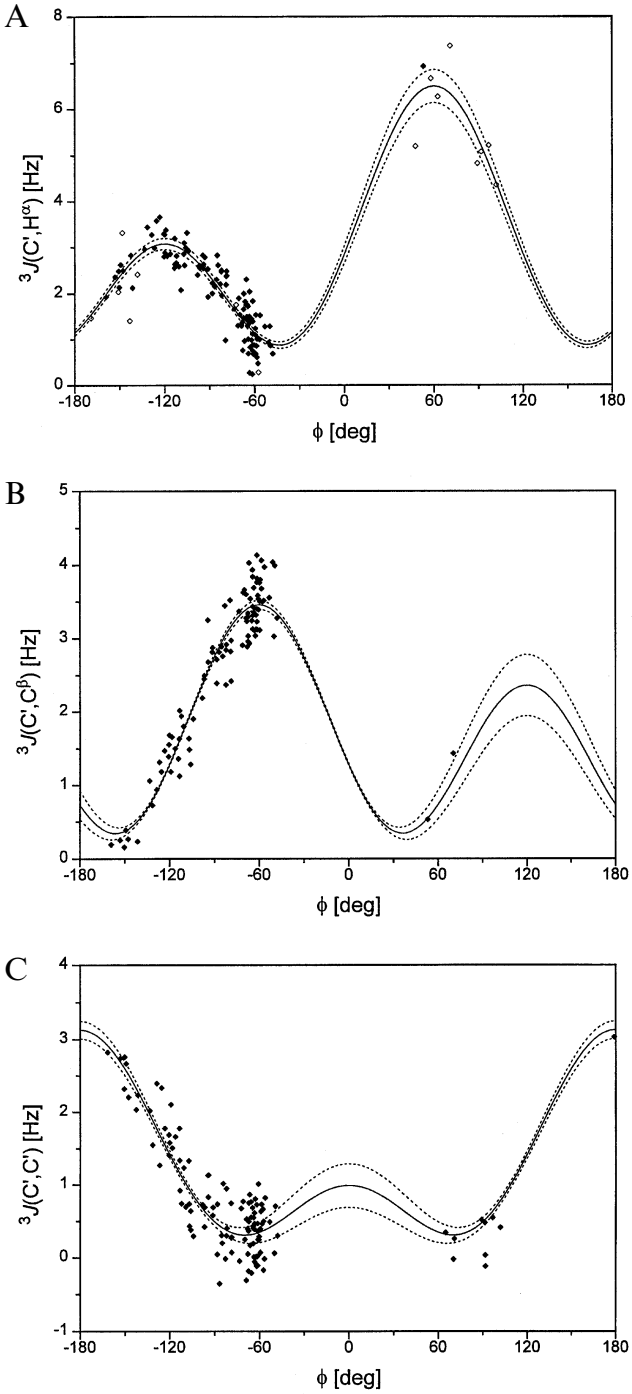

Fig. 5. Optimized Karplus curves based on (A) $^3J(C'_{i-1},H^\alpha_i)$, (B) $^3J(C'_{i-1},C^\beta_i)$ and (C) $^3J(C'_{i-1},C'_i)$ coupling constants measured for oxidized *Desulfovibrio vulgaris* flavodoxin (solid lines). Dashed lines indicate the Gaussian 3σ confidence boundaries obtained with 10 000 fits, randomly discarding (A) 13, (B) 10 and (C) 12 J-values in repetitive trials. Calibration points for glycine and non-glycine residues in part A are represented by open and filled diamonds, respectively. $^3J(C'_{i-1},H^\alpha_i)$ coupling constants extracted from the (H)NCAHA- and H(N)CA,CO-E.COSY spectra are not distinguished.

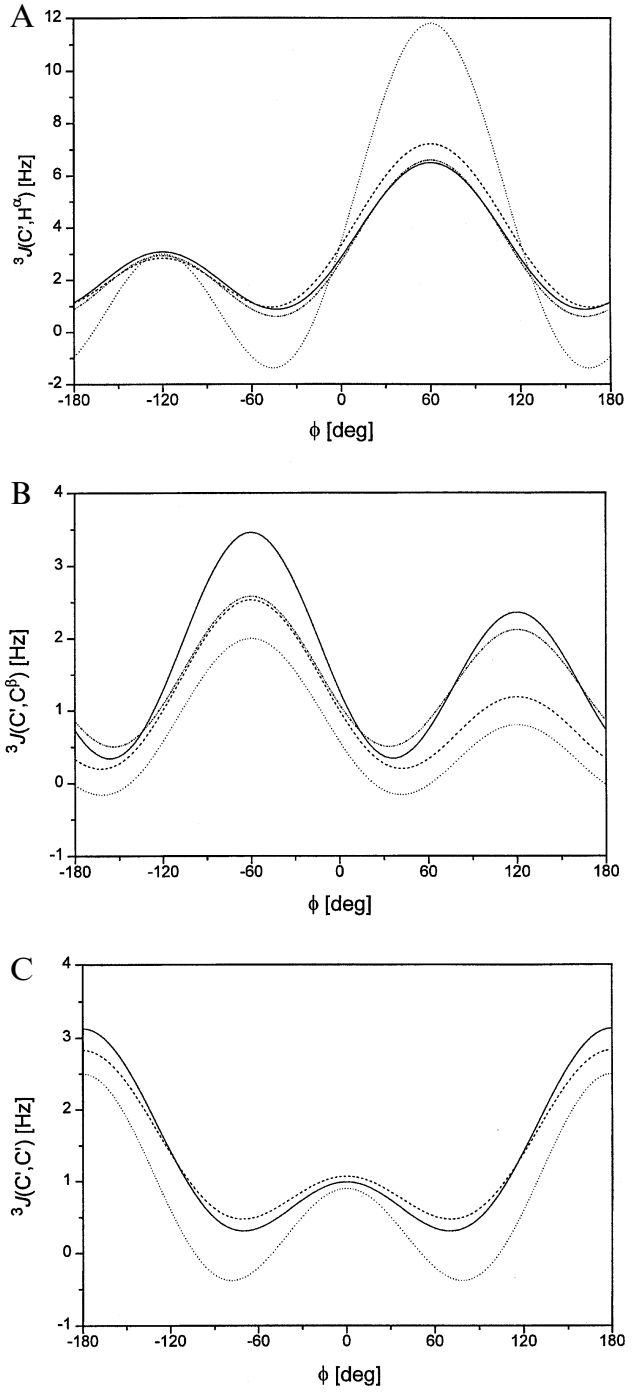

Fig. 6. Comparison of various empirical and theoretical Karplus parametrizations for (A) $^3J(C'_{i-1},H^\alpha_i)$, (B) $^3J(C'_{i-1},C^\beta_i)$ and (C) $^3J(C'_{i-1},C'_i)$. Curves obtained for flavodoxin in this study are represented by solid lines. The corresponding curves for ubiquitin are indicated by dashed lines and are taken from (A) Wang and Bax (1996), (B) Hu and Bax (1996b) and (C) Hu and Bax (1996a). Dotted lines denote the parametrizations given by (A) Bystrov et al. (1975) and (B,C) Solkan and Bystrov (1974). Karplus curves determined by Kao and Barfield (1985) are depicted by dot-dashed lines in parts A and B.

the precision of these values is lower than for non-glycine residues because the anyway lower signal-to-noise ratio of the (H)NCAHA is further diminished by the reduced efficiency in the final polarization transfer step for C^α methylene groups compared to methine species.

The least sensitive in the series of the H(N)CA,CO

experiments is the version in Fig. 1C because of both the relatively long period (≈27 ms) of transverse $^{13}C^{\alpha}$ magnetization present and the small-flip-angle pulse employed for the excitation of carbonyl spins. However, within an acceptable amount of measuring time, a signal-to-noise ratio sufficient for a reliable quantitative analysis of E.COSY patterns was obtained for all intraresidual cross peaks of the 16 kDa protein flavodoxin. Among the three coupling types, the smallest number of calibration points was available for the parametrization of the $^3J(C'_{i-1},C_i^{\beta})$ curve. This is merely due to a limitation of version B of the H(N)CA, CO experiment regarding the amino acid type. Besides proline and glycine residues, no values can be obtained for serines and threonines either as their β-carbon resonances are in the $^{13}C^{\alpha}$ region and are concomitantly excited by the band-selective carbon pulses, leading to an obliteration of the E.COSY multiplet pattern. As $^3J(C'_{i-1},C_i^{\beta})$ could only be measured for two residues with positive ϕ-angles, the corresponding curve is uncertain with respect to the position of the relative maximum at $\phi = +120°$. However, the couplings with absolute maxima in the positive ϕ-angle range (i.e. $^3J(C'_{i-1},H_i^{\alpha})$ and $^3J(H^N,C^{\beta})$) are considered to be much more useful for detecting such unusual conformations.

As expected from the similarity in the approaches, the Karplus equations resulting from H(N)CA,CO experiments applied to flavodoxin resemble those of Bax and coworkers better than those of Bystrov. The remaining deviations are attributed to the different experimental strategies. Spectra recorded in this study were of the E.COSY type, which give rise to frequency differences, while quantitative J correlation based on amplitude modulation was applied by Hu and Bax (1996a,b) for the measurement of the carbon–carbon coupling constants. The drawbacks of quantitative J correlation are that it is generally not possible to discriminate between positive and negative signs of the coupling constants and that only upper limits can be given for very small couplings. Depending on the sensitivity of the experiment actually used and the rotational correlation time of the protein sample, signals may be unobservable if the scalar interactions to be determined are weak. Precise $^3J(C'_{i-1},C'_i)$ values as small as 0.4 Hz determined in an HN(CO)CO experiment were reported for ubiquitin though. E.COSY-type methods are void of these complications. In flavodoxin, 86 out of 121 $^3J(C'_{i-1},C'_i)$ coupling constants are smaller than 1 Hz and 58 are below 0.5 Hz, including 12 negative values. For these reasons, our curve possesses a distinctively deeper minimum at $|\phi| \approx 70°$ than the one resulting from the HN(CO)CO-derived data of ubiquitin.

Very recently, Hu and Bax (1997) published a first experimental parametrization of the ϕ-torsional dependence of $^3J(C'_{i-1},C_i^{\beta})$ with A = 1.61, B = –0.66 and C = 0.26 Hz yielding absolute and secondary maxima of 2.53 Hz and 1.21 Hz, respectively. The $^3J(C'_{i-1},C_i^{\beta})$ curve determined in the present study on flavodoxin reaches an absolute maximum of 3.46 Hz at $\phi = -60°$, which is significantly (0.93 Hz) larger than with ubiquitin. The secondary maximum at $\phi = +120°$ of 2.36 Hz exceeds the ubiquitin curve by 1.15 Hz, which in fact is explained by rather poor sampling in the positive dihedral-angle range in both studies and is not considered significant. However, comparison of the expected mean coupling constants due to complete angular rotation yields 1.64 and 1.07 Hz in the flavodoxin and ubiquitin cases, respectively. Given that the distribution of secondary structure elements is similar in both proteins, it is interesting that experimental J values range from approximately 0.25 to 2.8 Hz in ubiquitin while our values are as large as 4.15 Hz. The pronounced scatter in the larger $^3J(C'_{i-1},C_i^{\beta})$ values indicative of α-helical segments is consistently observed also in flavodoxin $^3J(C'_{i-1},H_i^{\alpha})$ and $^3J(C'_{i-1},C'_i)$ data. However, ubiquitin exhibits less divergent data at least for $^3J(C'_{i-1},C_i^{\beta})$ and $^3J(C'_{i-1},C'_i)$ values (Hu and Bax, 1996a,1997). This hints at possible differences in the experimental approach. Relaxation might cause rapid $^{13}C^{\beta}$ spin flips during the respective de- and rephasing periods in the HN(CO)C experiment (Hu and Bax, 1997), but the effect is too small to explain the relatively large deviation between the two curves. Spectrum processing and evaluation is also critical to the results obtained. However, with respect to our procedures, we are tempted to rely on direct evidence from the parallel measurements of $^3J(C'_{i-1},H_i^{\alpha})$ and $^3J(C'_{i-1},C'_i)$ coupling constants, which agree well with other results. Last but not least, the sample conditions might differ considerably.

No attempts were made in the present study to account for, firstly, possible differences between crystallographic ϕ-angles of flavodoxin and those present in solution and, secondly, the neglect of motional averaging inherent to the empirical determination of Karplus coefficients (Brüschweiler and Case, 1994).

Conclusions

A method has been introduced which allows measuring three types of vicinal J coupling constants related to the ϕ torsional angle in polypeptides, with only slight modifications in the experimental set-up. Application to flavodoxin yielded empirical calibrations of the respective Karplus curves to obtain accurate angle constraints in protein structure determination. While the $^3J(C'_{i-1},H_i^{\alpha})$ coupling constants accessed are useful for the recognition of unusual positive ϕ-angles, the $^3J(C'_{i-1},C_i^{\beta})$ and $^3J(C'_{i-1},C'_i)$ couplings exhibit large, opposite variations in the –140° to –70° and –160° to –90° ranges, respectively. A knowledge of the interresidual $^{13}C'$ three-bond couplings therefore supplements the information available from the three complementary intraresidual scalar interactions involving amide protons. In particular, these methods are proposed

for the determination of the $^{13}C,^{13}C$ couplings in larger, deuterated proteins.

Acknowledgements

This work was supported by the Deutsche Forschungsgemeinschaft under Grant Ru145/11-2. We gratefully acknowledge support from Prof. Stephen G. Mayhew (Department of Biochemistry, University College Dublin) with the expression and labelling of the *D. vulgaris* flavodoxin. Dr. Martin Walsh (EMBL, Hamburg) kindly provided the refined X-ray coordinates of oxidized flavodoxin prior to publication.

References

Bax, A., Vuister, G.W., Grzesiek, S., Delaglio, F., Wang, A.C., Tschudin, R. and Zhu, G. (1994) *Methods Enzymol.*, **239**, 79–105.

Biamonti, C., Rios, C.B., Lyons, B.A. and Montelione, G.T. (1994) *Adv. Biophys. Chem.*, **4**, 51–120.

Boyd, J., Soffe, N., John, B., Plant, D. and Hurd, R. (1992) *J. Magn. Reson.*, **98**, 660–664.

Brüschweiler, R. and Case, D.A. (1994) *J. Am. Chem. Soc.*, **116**, 11199–11200.

Bystrov, V.F., Gavrilov, Yu.D. and Solkan, V.N. (1975) *J. Magn. Reson.*, **19**, 123–129.

Bystrov, V.F. (1976) *Prog. NMR Spectrosc.*, **10**, 41–81.

Case, D.A., Dyson, H.J. and Wright, P.E. (1994) *Methods Enzymol.*, **239**, 392–416.

Davis, A.L., Keeler, J., Laue, E.D. and Moskau, D. (1992) *J. Magn. Reson.*, **98**, 207–216.

DeMarco, A., Llinás, M. and Wüthrich, K. (1978a) *Biopolymers*, **17**, 617–636.

DeMarco, A., Llinás, M. and Wüthrich, K. (1978b) *Biopolymers*, **17**, 637–650.

DeMarco, A., Llinás, M. and Wüthrich, K. (1978c) *Biopolymers*, **17**, 2727–2742.

DeMarco, A. and Llinás, M. (1979) *Biochemistry*, **18**, 3846–3854.

Eberstadt, M., Gemmecker, G., Mierke, D.M. and Kessler, H. (1995) *Angew. Chem., Int. Ed. Engl.*, **34**, 1671–1695.

Emsley, L. and Bodenhausen, G. (1990) *Chem. Phys. Lett.*, **165**, 469–476.

Fischman, A.J., Live, D.H., Wyssbrod, H.R., Agosta, W.C. and Cowburn, D. (1980) *J. Am. Chem. Soc.*, **102**, 2533–2539.

Griesinger, C., Sørensen, O.W. and Ernst, R.R. (1985) *J. Am. Chem. Soc.*, **107**, 6394–6396.

Griesinger, C., Sørensen, O.W. and Ernst, R.R. (1986) *J. Chem. Phys.*, **85**, 6837–6852.

Griesinger, C., Sørensen, O.W. and Ernst, R.R. (1987) *J. Magn. Reson.*, **75**, 474–492.

Grzesiek, S. and Bax, A. (1992) *J. Magn. Reson.*, **96**, 432–440.

Grzesiek, S. and Bax, A. (1993a) *J. Am. Chem. Soc.*, **115**, 12593–12594.

Grzesiek, S. and Bax, A. (1993b) *J. Biomol. NMR*, **3**, 627–638.

Grzesiek, S., Vuister, G.W. and Bax, A. (1993) *J. Biomol. NMR*, **3**, 487–493.

Hansen, P.E., Feeney, J. and Roberts, G.C.K. (1975) *J. Magn. Reson.*, **17**, 249–261.

Harbison, G.J. (1993) *J. Am. Chem. Soc.*, **115**, 3026–3027.

Hoch, J.C., Dobson, C.M. and Karplus, M. (1985) *Biochemistry*, **24**, 3831–3841.

Hosur, R.V., Ravi Kumar, M. and Sheth, A. (1985) *J. Magn. Reson.*, **65**, 375–381.

Hu, S.-J. and Bax, A. (1996a) *J. Am. Chem. Soc.*, **118**, 8170–8171.

Hu, S.-J. and Bax, A. (1996b) *XVIIth International Conference on Magnetic Resonance in Biological Systems*, August 18–23, 1996, Keystone, U.S.A., poster TP21.

Hu, S.-J. and Bax, A. (1997) *J. Am. Chem. Soc.*, **119**, 6360–6368.

Kao, L.-F. and Barfield, M. (1985) *J. Am. Chem. Soc.*, **107**, 2323–2330.

Karplus, M. (1959) *J. Chem. Phys.*, **30**, 11–15.

Karplus, M. (1963) *J. Am. Chem. Soc.*, **85**, 2870–2871.

Kay, L.E., Xu, G.Y. and Yamazaki, T. (1994) *J. Magn. Reson.*, **A109**, 129–133.

Knauf, M., Löhr, F., Blümel, M., Mayhew, S.G. and Rüterjans, H. (1996) *Eur. J. Biochem.*, **238**, 423–434.

Krishnamurthy, V.V. (1995) *J. Magn. Reson.*, **A114**, 88–91.

Li, Y.-C. and Montelione, G.T. (1993) *J. Magn. Reson.*, **B101**, 315–319.

Löhr, F. and Rüterjans, H. (1995) *J. Biomol. NMR*, **5**, 25–36.

Löhr, F. and Rüterjans, H. (1996) *13th European Experimental NMR Conference*, May 19–24, 1996, Paris, France, poster p80.

Löhr, F. and Rüterjans, H. (1997) *J. Am. Chem. Soc.*, **119**, 1468–1469.

Ludvigsen, S., Andersen, K.V. and Poulsen, F.M. (1991) *J. Mol. Biol.*, **217**, 731–736.

Marion, D., Ikura, M. and Bax, A. (1989a) *J. Magn. Reson.*, **84**, 425–430.

Marion, D., Ikura, M., Tschudin, R. and Bax, A. (1989b) *J. Magn. Reson.*, **85**, 393–399.

Nagayama, K. (1986) *J. Magn. Reson.*, **66**, 240–249.

Norwood, T.J. (1993) *J. Magn. Reson.*, **A101**, 109–112.

Norwood, T.J. and Jones, K. (1993) *J. Magn. Reson.*, **A104**, 106–110.

Pardi, A., Billeter, M. and Wüthrich, K. (1984) *J. Mol. Biol.*, **180**, 741–751.

Piotto, M., Saudek, V. and Sklenář, V. (1992) *J. Biomol. NMR*, **2**, 661–665.

Press, W.H., Flannery, B.P., Teukolsky, S.A. and Vetterling, W.T. (1989) *Numerical Recipes*, Cambridge University Press, Cambridge, U.K.

Schmidt, J.M., Ernst, R.R., Aimoto, S. and Kainosho, M. (1995) *J. Biomol. NMR*, **6**, 95–105.

Shaka, A.J., Barker, P.B. and Freeman, R. (1985) *J. Magn. Reson.*, **64**, 547–552.

Shaka, A.J., Lee, C.J. and Pines, A. (1988) *J. Magn. Reson.*, **77**, 274–293.

Solkan, V.N. and Bystrov, V.F. (1974) *Izv. Akad. Nauk SSSR, Ser. Khim.*, 1308–1313.

Stockman, B.J., Richardson, T.E. and Swenson, R.P. (1994) *Biochemistry*, **33**, 15298–15308.

Stonehouse, J., Shaw, G.L., Keeler, J. and Laue, E.D. (1994) *J. Magn. Reson.*, **A107**, 178–184.

Szyperski, T., Braun, D., Fernández, C., Bartels, C. and Wüthrich, K. (1995) *J. Magn. Reson.*, **B108**, 197–203.

Vuister, G.W. and Bax, A. (1993) *J. Am. Chem. Soc.*, **115**, 7772–7777.

Wang, A.C. and Bax, A. (1995) *J. Am. Chem. Soc.*, **117**, 1810–1813.

Wang, A.C. and Bax, A. (1996) *J. Am. Chem. Soc.*, **118**, 2483–2494.

Watenpaugh, K.D., Sieker, L.C., Jensen, L.H., LeGall, J. and Dubourdieu, M. (1972) *Proc. Natl. Acad. Sci. USA*, **69**, 3185–3188.

Watenpaugh, K.D., Sieker, L.C. and Jensen, L.H. (1973) *Proc. Natl. Acad. Sci. USA*, **70**, 3857–3860.

Watt, W., Tulinsky, A., Swenson, R.P. and Watenpaugh, K.D. (1991) *J. Mol. Biol.*, **218**, 195–208.

Zhu, G. and Bax, A. (1990) *J. Magn. Reson.*, **90**, 405–410.